Effect of mineral heterogeneity on fracture dissolution in carbonate-rich caprocks during subsurface CO_2 injection

H Fazeli, M Nooraiepour, M Masoudi, H Hellevang [1,*]
[1] Department of Geosciences, University of Oslo, P.O. Box 1047 Blindern, 0316 Oslo, Norway
* Correspondence: mohammad.nooraiepour@geo.uio.no

Introduction

Geological CO_2 storage and CCS have a crucial role in reducing CO_2 emission and therefore mitigating climate change. One of the prerequisites for the selection of CO_2 storage sites is the existence of a low-permeability caprock preventing potential CO_2 leakage and migration from the storage reservoir. Presence of fractures in the caprock can adversely affect the sealing capacity of caprocks (Nooraiepour et al., 2018a). Chemical interactions between CO_2, brine, and caprock-forming minerals can cause fracture evolution, which results in changes in the transmissivity of fractures within the sealing layers. Parameters such as flow rate, solution chemistry, initial geometry or fracture aperture, and mineral heterogeneity can influence reaction-induced fracture alterations (Fazeli et al., 2018, 2019). In the majority of previous experimental studies, x-ray computed tomography was deployed to investigate the micro-scale features, such as the effect of mineral heterogeneity on fracture evolution. In this work, we introduced a microfluidic approach at reservoir conditions for this purpose. Most of the microfluidic experiments are performed with chips made of glass, silicon, or polymeric materials. In geoscience-related processes, however, it is vital to use geomaterial substrates because the fluid-rock geochemical interactions have crucial roles in the processes. Moreover, subsurface processes involve high-pressure and high-temperature (HPHT) conditions. There are not many microfluidic techniques that have been adapted for geomaterial substrates and HPHT conditions (Nooraiepour et al., 2018b; Fazeli et al., 2020). To our knowledge, the HPHT geomaterial microfluidic devices have not yet been used to investigate the geochemical interactions between reactive fluids and rock-forming minerals.

In the present work, we investigate the effect of mineral heterogeneity on fracture geometry evolution when CO_2-rich brine is flowing through a single fracture scribed on different carbonate-rich caprock samples. The rock samples have different carbonate contents and different levels of mineral heterogeneities. They can represent carbonate-rich caprocks such as some intervals of the Upper Jurassic (Kimmeridgian) Draupne shales, the caprock for Smeaheia CO_2 storage in Norway. The microfluidic instrument allows continuous observation of fracture morphology during the experiments. The effluent fluid chemistry was also analyzed to further evaluate the fluid reactivity in the fractures and the sample-scale carbonate dissolution rate.

Materials and Methods

Micromodels and experimental setup. As shown in Table 1, a total of four representative specimens of carbonate-rich caprocks were used to prepare the micromodels. Three experiments were performed on natural core samples, and one test was carried out on a laboratory-made rock specimen. The post-experiment images of the microfluidic substrates are presented in Figure 1. The natural caprock samples had the following characteristics: sample A: low mineral heterogeneity, sample B: high mineral heterogeneity, and sample C: high mineral heterogeneity impregnated with epoxy resin under vacuum (Table 1 and Fig. 1a-c). These microfluidic substrates have high calcite content, and impregnating sample B with epoxy resin introduced one fully non-reactive phase into the specimen, which helped us study the subsequent effect on fracture dissolution and geometry evolution. The laboratory-made rock specimen (sample D) was prepared by mechanical compaction of brine-saturated mineral aggregates. The details of laboratory mechanical compaction were presented in Nooraiepour et al. (2017; 2019). The laboratory-made specimen comprises 50% carbonate (mostly calcite) and 50% reconstituted aggregates of organic-rich shale of the Kimmeridgian Draupne Formation. The main difference between natural and synthetic samples is that the laboratory-made sample is carbonate mixed with shale, while the natural samples do not have shale content. For HPHT reactive transport experiments, at the University of Oslo, we have

Table 1 *Geomaterial microfluidic substrates*

Sample	Geomaterial Substrate
A	Homogeneous carbonate-rich
B	Heterogeneous carbonate-rich
C	Sample B, impregnated with epoxy resin
D	Heterogeneous carbonate-rich organic shale

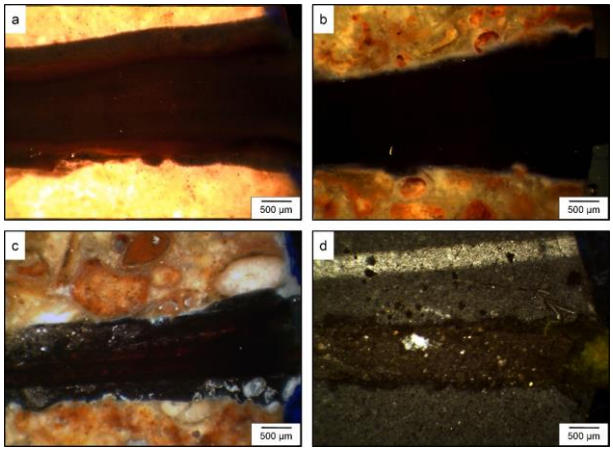

Figure 1 *Post-experiment state of fractured-geomaterial microfluidic substrates. (a) sample A, (b) sample B, (c) sample C, and (d) sample D. For pre-experiment images of samples A, C, and D, see Fazeli et al. (2020).*

designed and manufactured a stainless-steel pressure vessel to accommodate geomaterial micromodels. For detailed description, refer to Fazeli et al. (2020) and Nooraiepour et al. (2018b). The microfluidic pressure vessel was then connected to an AFS-200 core flooding system driving the reactive solution from the reservoir and through the sample with a high-precision dual-piston pump (Moghadam et al., 2019).

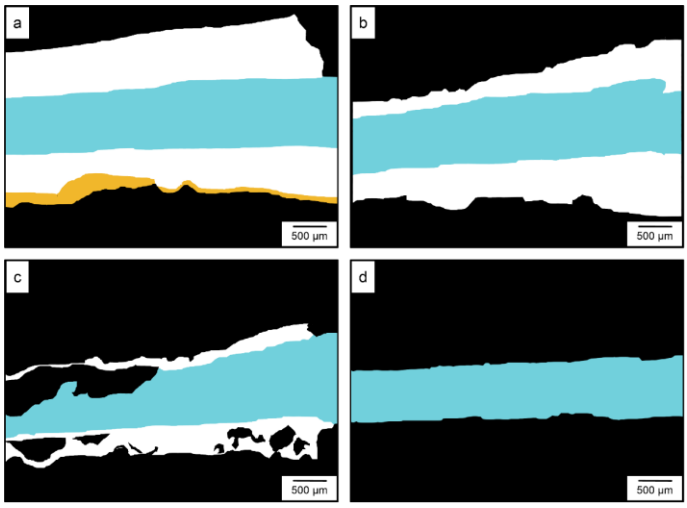

Figure 2 *Fracture geometry evolution for samples (a) A (b) B, (c) C, and (d) D. It shows the microfluidic substrate where black indicates the rock matrix; light blue shows the initial fracture channel; white refers to the dissolved matrix after exposure to the CO_2-charged water. The yellow color in (a) represents a less-reactive band.*

Experimental procedure. To prepare the carbonated water, we stored 1000 ml of deionized water of Milli-Q quality (hereafter DI-water) in a fluid transfer vessel and then introduced gaseous CO_2 at 5 MPa and 20°C. A tracker dye (red and yellow color) was added to the DI-water to track fracture geometry evolution during the experiments better. The microfluidic specimens were initially saturated with the DI-water. We conducted experiments at a constant flow rate regime at 4 MPa back-pressure, 20°C temperature, and two flow rates: (a) 7 days at 0.025 cm^3/min and (b) 3 days at 0.1 cm^3/min. The experiments, hence, lasted for ten days. The test fluid after reacting with the substrates was collected in a fluid sampling container and analyzed at one-day intervals.

Performed analyses. The injected fluid (before and after reaction) was analyzed for Ca^{2+} concentration using a Dionex ICS-2000 ion chromatography system. To track changes in fracture geometry, we digitally recorded the experiment using a Nikon SMZ stereomicroscope equipped with a high-resolution digital camera. To enhance contrast and reduce image noise, we applied several filters such as edge-preserving nonlocal-means algorithm on the raw 2D optical images. The experimental images were then imported in MATLAB and binarized for further analyses. To refine the fracture boundaries and better differentiate segmented components, supervised-identification was also implemented.

Results and Discussion

Fracture geometry alteration. When CO_2-rich brine flows through the fracture, it dissolves calcite and causes reaction-induced changes in fracture geometry. Fracture alteration depends on mineral types and heterogeneity. Figure 2 shows the fracture geometry in day 1 and 10 for different samples. For sample A, we can see a smooth fracture wall dissolution, especially for the upper fracture wall (Figs. 1a & 2a). For the lower fracture wall, after some calcite dissolution, the reacting fluid reaches a less reactive band that creates some roughness. For sample B, the degree of fracture roughness after the test is higher compared to sample A, yet lower than sample C (Figs. 1b & 2b). For sample C, heterogeneous impregnated sample, after the dissolution of calcite, some of the less reactive grains and epoxy remain unreacted, and the fracture roughness increases over time. This effect is evident in Figure 2(c), where the black spots near the inlet indicate these non-reactive epoxies. For the synthetic carbonate-rich organic shale (Figs. 1d & 2d), however, no evident macroscopic alteration could be observed during the experimental time scale.

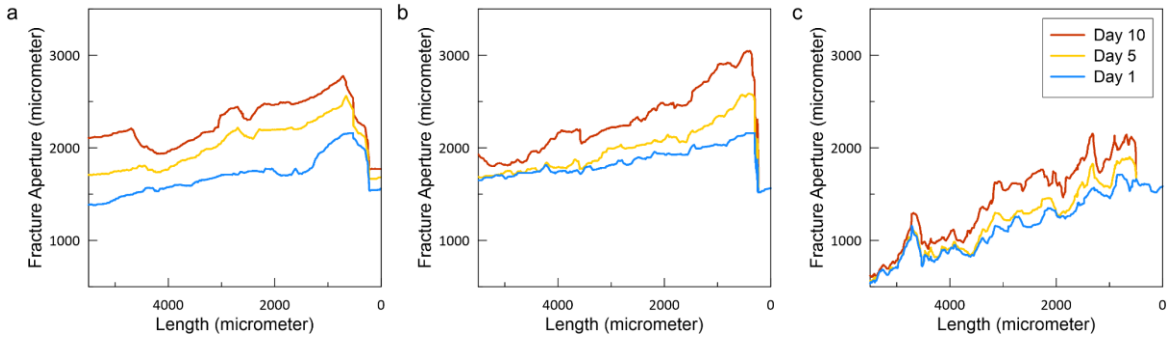

Figure 3 *Temporal evolution of the fracture aperture for samples (a) A, (b) B, and (c) C. The zero in x-axis shows the channel inlet. No macroscopic changes were observed for sample D. For the evolution of fracture aperture and geometry at more time steps (samples A and C), see Fazeli et al. (2020).*

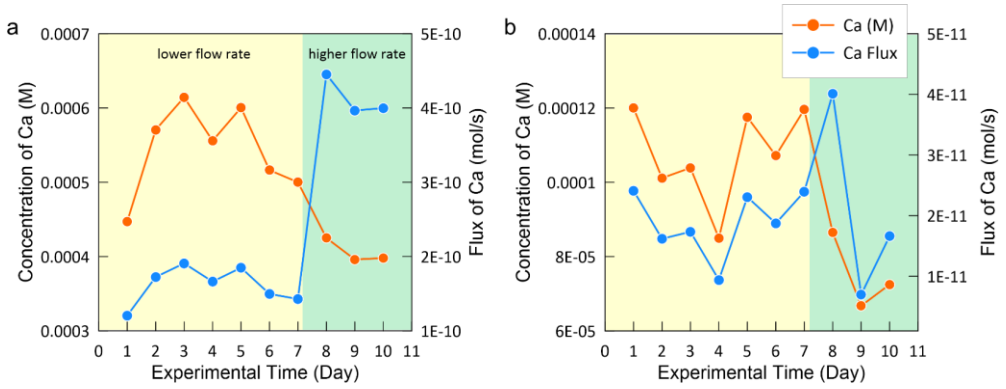

Figure 4 *Comparison of temporal changes in effluent concentration and calculated flux of Ca^{2+} for samples (a) C and (b) D. Flow rate: 7 days at 0.025 cm^3/min and then 3 days at 0.1 cm^3/min. For the evolution of Ca for other samples, see Fazeli et al. (2020).*

Figure 3 displays the temporal evolution of fracture aperture for samples A, B, and C during the ten-days of the experiments. The sample D is not included as the alterations were below the resolution of the optical microscope. As shown in Figure 3, the temporal fracture evolutions for sample A are smoother compared to the contours representing the heterogeneous samples. Figure 3c illustrates very rough contours for sample C due to the presence of slow-reacting minerals and epoxy resins. As Figure 3 depicts for sample A, the highest aperture increase due to dissolution can be seen in the regions near the inlet where the pH of the solution is lower compared to the downstream areas. Near the outlet, the injected solution has been buffered due to the reactions between the low-pH solution and calcite. For the samples B and C (Fig. 3b-c), the rate of aperture change becomes lower as we move towards the outlet. In Figure 3c, it can be observed that the aperture values at the outlet are very similar and that no jump in aperture values is detectable. For sample A (Fig. 3a), however, there is a clear difference between aperture values measured at different days, and even close to the outlet. It is due to the absence of less- and non-reactive minerals in the rock matrix.

Effluent chemistry. The effluent Ca^{2+} concentration was measured to examine the rate of calcite dissolution. As Figure 4(a) shows for sample C, Ca^{2+} fluctuates a bit, but the overall trend shows a decreasing behavior, although the concentration at day 7 is higher than Ca^{2+} concentration for day 1. Contrary to sample C, for sample D Ca^{2+} declines with time from day 1 (0.00012) to day 2 (0.0001), and then fluctuating in this range until day 7 (Fig. 4b). The initial decrease in Ca^{2+} observed in sample D might be due to the low amount of calcite accessible to the reactive fluid. Figure 5 shows how calcite, with the content of ~50%, is armored by clay and quartz. This armoring results in less available calcite surface for the reaction after day 1. Clay and quartz in the fine-grained shale samples can cover calcite surfaces that leads to more limited diffusion in the porous layers around the fracture (Fig. 5d). In sample D, therefore, a limited reaction occurs while in the coarse-grained carbonate rocks, the diffusion in the altered layer is not as limited as that of sample D (Fig. 5a-c).

As temporal changes in Ca^{2+} in the low injection flow rate shows (Fig. 4), the general behavior in all cases is that calcite dissolution decreases over time. At low pH, calcite dissolution is limited by transport processes. For sample A, the reduction in calcite dissolution can be attributed to the diffusion boundary layer that forms near the fracture walls. This layer can decrease the calcite dissolution rate by limiting the transport of reactants and products. For samples B and C, the interaction between low-pH solution and minerals with different reactivities such as calcite, clay, and quartz can create altered layers where the mass transfer is limited to diffusion. The reactants and products, hence, are transported by diffusion in the altered layer, and the

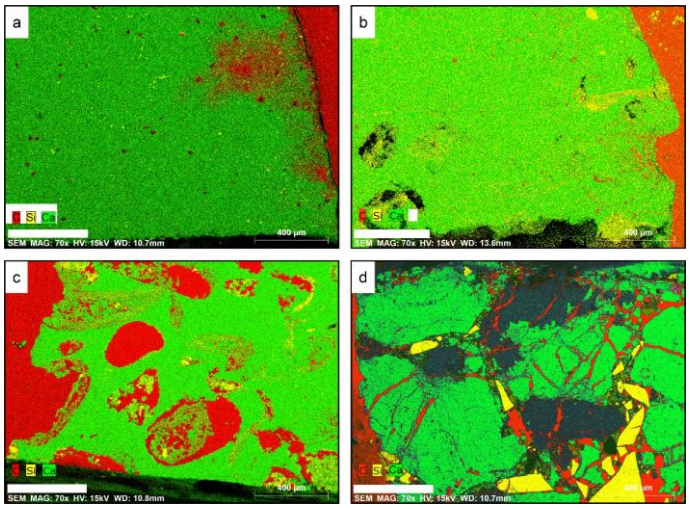

Figure 5 *Elemental phase mapping of the fractured microfluidic substrates. Samples (a) A, (b) B, (c) C, and (d) D. Ca refers to calcite, Si to silicate minerals, and C to epoxy resin. It shows the before-reaction state of the rock matrix adjacent to the fracture.*

dissolution rate will therefore decrease. When the injection flow rate increases, a decrease in Ca^{2+} can be observed for all cases. The calcium fluxes, defined as $F_{Ca} = flow\ rate \times (Ca^{2+}_{out} - Ca^{2+}_{in})$, however, increases for all the samples from day 7 to 8. The increase in flow rate is so high that it can overcome the decrease in flow rate due to aperture increase. The other reason for the increase in F_{Ca} can be due to the increase in calcite dissolution.

Conclusions

A new experimental approach was used to investigate the fracture geometry evolution of artificially fractured carbonate-rich caprock samples having different levels of mineral heterogeneity. The study benefited from a recently developed geomaterial microfluidic device that can operate in high-pressure high-temperature conditions and uses the real rock specimens as the substrate.

In carbonate-rich samples without shale, the fracture dissolution is more pronounced and enhanced at the sample inlet due to exposure to the solution with lower pH. The dissolution pattern for the homogeneous sample (A) demonstrated a smooth fracture wall dissolution, whereas for the more heterogeneous samples (B and C) a rough fracture wall formed after calcite dissolution due to the presence of slow-reacting minerals and non-reactive epoxy-based materials. The decreasing trend in effluent Ca concentrations for all samples, when the injection flow rate is constant, showed that the diffusion limitation in mass transfer might affect the dissolution rate of calcite. In sample A, the mass transfer is limited to diffusion in the boundary layer formed near the fracture walls, while for heterogeneous samples (B and C), the diffusion limitation occurs in the altered layers created after calcite dissolution. The effluent Ca concentration of carbonate-rich organic shale sample confirmed the dissolution of calcite, but no macroscopic fracture alteration was recorded during the ten-day experiment. This shows that in shale samples where the carbonate minerals, particularly calcite, are armored with other slow reacting minerals such as clays, the rate of fracture geometry evolution will be prolonged which might be a positive point for the caprock integrity. However, the confirmed fluid-rock geochemical interactions within the shaly sample (D) in a short time frame calls for further investigations on the consequent impacts on geomechanical-hydrological properties of caprock samples for more extended periods relevant for subsurface CO_2 storage. It is of high importance for some intervals of the Upper Jurassic Draupne shales, the caprock for Smeaheia CO_2 storage site in offshore Norway.

Acknowledgements

This publication has been produced with support from the “solid and salt precipitation kinetics during CO2 injection into reservoir” project (funded by Norway Grants under grant number UMO-2019/34/ H/ST10/00564 through the GRIEG Programme).

References

Fazeli, H., Nooraiepour, M., and Hellevang, H. [2020]. Microfluidic study of fracture dissolution in carbonate-rich caprocks subjected to CO_2-charged brine. *Industrial & Engineering Chemistry Research*.

Fazeli, H., Patel, R. A., Ellis, B. R., and Hellevang, H. [2019]. Three-dimensional pore-scale modeling of fracture evolution in heterogeneous carbonate caprock subjected to CO_2-enriched brine. *Environmental Science & Technology*, 53(8), 4630–4639.

Fazeli, H., Patel, R., and Hellevang, H. [2018]. Effect of pore-scale mineral spatial heterogeneity on chemically induced alterations of fractured rock: A Lattice Boltzmann study. *Geofluids*, p. 28.

Moghadam, J. N., Nooraiepour, M., Hellevang, H., Mondol, N. H., and Aagaard, P. [2019]. Relative permeability and residual gaseous CO_2 saturation in the Jurassic Brentskardhaugen Bed sandstones, Wilhelmøya Subgroup, western central Spitsbergen, Svalbard. *Norwegian Journal of Geology*, 99(2), 1–12.

Nooraiepour, Mohammad, Mondol, N. H., and Hellevang, H. [2019]. Permeability and physical properties of semi-compacted fine-grained sediments – A laboratory study to constrain mudstone compaction trends. *Marine and Petroleum Geology*, 102, 590-603.

Nooraiepour, M, Bohloli, B., Park, J., Sauvin, G., Skurtveit, E., and Mondol, N. H. [2018a]. Effect of brine- CO_2 fracture flow on velocity and electrical resistivity of naturally fractured tight sandstones. *Geophysics*, 83:1.

Nooraiepour, M., Fazeli, H., Miri, R., and Hellevang, H. [2018b]. Effect of CO_2 phase states and flow rate on salt precipitation in shale caprocks- A microfluidic study. *Environmental Science and Technology*, 52(10), 6050-6060.

Nooraiepour, Mohammad, Mondol, N. H., Hellevang, H., and Bjørlykke, K. [2017]. Experimental mechanical compaction of reconstituted shale and mudstone aggregates: Investigation of petrophysical and acoustic properties of SW Barents Sea cap rock sequences. *Marine and Petroleum Geology*, 80, 265-292.